

## Article

# Flexible, Biocompatible PET Sheets: A Platform for Attachment, Proliferation and Differentiation of Eukaryotic Cells

Soumen Samanta<sup>1</sup>, Diana Gaad<sup>2,†</sup>, Eva Cabet<sup>3,4,\*</sup>, Alain Lilienbaum<sup>3</sup>, Ajay Singh<sup>1</sup>, Dinesh K. Aswal<sup>1</sup> and Mohamed M. Chehimi<sup>2,\*</sup> 

<sup>1</sup> Technical Physics Division, Bhabha Atomic Research Centre (BARC), Mumbai 400085, India; soumen.samanta@gmail.com (S.S.); ajay@barc.gov.in (A.S.); dkaswal@yahoo.com (D.K.A.)

<sup>2</sup> Université de Paris, ITODYS, UMR CNRS 7086, 15 rue J-A de Baïf, 75013 Paris, France; gaad.diana@hotmail.fr

<sup>3</sup> Université de Paris, BFA, UMR CNRS 8251, 5 rue Marie-Andrée Lagroua Weill-Halle, 75013 Paris, France; alain.lilienbaum@univ-paris-diderot.fr

<sup>4</sup> Université de Paris, UMR CNRS 8236, LIED Laboratoire Interdisciplinaire des Energies de Demain, 75013 Paris, France

\* Correspondence: eva.cabet@u-paris.fr (E.C.); mohamed.chehimi@cnrs.fr (M.M.C.)

† Current address: Assystem, 92400 Courbevoie, France.

**Abstract:** Transparent, flexible, biaxially oriented polyethylene terephthalate (PET) sheets were modified by bioactive polymer-fibronectin top layers for the attachment of cells and growth of muscle fibers. Towards this end, PET sheets were grafted with 4-(dimethylamino)phenyl (DMA) groups from the in situ generated diazonium cation precursor. The arylated sheets served as macrohydrogen donors for benzophenone and the growth of poly(2-hydroxy ethyl methacrylate) (PHEMA) top layer by surface-confined free radical photopolymerization. The PET-PHEMA sheets were further grafted with fibronectin (FBN) through the 1,1-carbonyldiimidazole coupling procedure. The bioactive PET-PHEMA-I-FBN was then employed as a platform for the attachment, proliferation and differentiation of eukaryotic cells which after a few days gave remarkable muscle fibers, of ~120 µm length and ~45 µm thickness. We demonstrate that PET-PHEMA yields a fast growth of cells followed by muscle fibers of excellent levels of differentiation compared to pristine PET or standard microscope glass slides. The positive effect is exacerbated by crosslinking PHEMA chains with ethylene glycol dimethacrylate at initial HEMA/EGDA concentration ratio = 9/1. This works conclusively shows that in situ generated diazonium salts provide aryl layers for the efficient UV-induced grafting of biocompatible coating that beneficially serve as platform for cell attachment and growth of muscle fibers.

**Keywords:** eukaryotic cells; cell adhesion; muscle fibers; fibronectin; flexible supports; biocompatible polymers; diazonium salts; surface modification



**Citation:** Samanta, S.; Gaad, D.; Cabet, E.; Lilienbaum, A.; Singh, A.; Aswal, D.K.; Chehimi, M.M. Flexible, Biocompatible PET Sheets: A Platform for Attachment, Proliferation and Differentiation of Eukaryotic Cells. *Surfaces* **2021**, *4*, 306–322. <https://doi.org/10.3390/surfaces4040026>

Academic Editor: Gaetano Granozzi

Received: 15 November 2021

Accepted: 8 December 2021

Published: 10 December 2021

**Publisher's Note:** MDPI stays neutral with regard to jurisdictional claims in published maps and institutional affiliations.



**Copyright:** © 2021 by the authors. Licensee MDPI, Basel, Switzerland. This article is an open access article distributed under the terms and conditions of the Creative Commons Attribution (CC BY) license (<https://creativecommons.org/licenses/by/4.0/>).

## 1. Introduction

The development of flexible surfaces is essential to create soft spatial topologies that allow one to study mechanical strains on cells, or to graft cells into moving organs subjected to topological constraints, like muscles, for example [1–3]. Indeed, biomaterials play a major role in modern medicine; they can be employed as part of reconstructive implants [4], implanted sensing objects [5], and a system for site-specific drug delivery [6]. Advances in biomaterials have led to non-toxic implants as well as those that are specifically designed to elicit particular functions within the host [7,8].

Extracellular matrix (ECM)-based tissue engineering strategies are already successfully employed clinically for the regeneration of a range of different tissues [9], including heart valves [10], trachea [11], muscles [12], tendons [13], and abdominal walls [14]. Successful clinical application of specifically designed implants has been thus reported in cardiovascular, gastrointestinal, and breast reconstructive surgery [15].

Eucaryotic cells that make up implants normally grow in multicellular organisms surrounded by a specific molecular environment, the extracellular matrix [16,17]. ECM is a dynamic and complex environment characterized by biophysical, mechanical and biochemical properties specific for each tissue. The ECM consists of a complex assembly of several proteins and polysaccharides the precise composition of which varies from tissue to tissue. The primary components include insoluble fibrous structural proteins (i.e., collagens, laminins, fibronectin, vitronectin, and elastin), proteoglycans, and specialized proteins (i.e., growth factors, small matricellular proteins, and small integrin-binding glycoproteins) [18,19]. ECM is thus critically important for many cellular processes including growth, differentiation, survival, and morphogenesis [20,21].

Flexible substrates are not only of importance to biomedical research and development but find also numerous other applications pertaining to thermoelectric organic materials [22], sensors [23], and dye-sensitized solar cells [24], to name but a few. However, regardless of the application, substrates usually require surface modifications, particularly when they are intended to support reactive and functional compounds [25], polymers [26], biomacromolecules [27], and living cells [28]. Towards this end, several surface engineering strategies are currently investigated in view of designing robust devices. Particularly, over recent years, time and efforts were spent on the surface modification of a range of substrates by ultrathin reactive and functional polymer films [29]. One of the elegant strategies to attach polymers to surfaces is through the modern approach employing diazonium coupling agents [30]. This strategy is now accepted and explored by several laboratories around the globe [25,31–33]. However, whilst it is currently applied to numerous materials such as metals, carbon, and semi-conductors, only a few reports considered the modification of plastic substrates by aryl diazonium salts for biomedical purposes. In this regard, Ben Slama et al. [34] prepared copolymer–silver grafts on ITO for anti-bacterial applications, whereas Mahjoubi et al. [35] have used diazonium salts for the surface phosphonation of polyetheretherketone (PEEK) in order to design new PEEK-based orthopedic implants.

In the present work, we have used polyethylene terephthalate sheets, modified with the diazonium compound of *N,N*-dimethyl-*p*-phenylenediamine (PET-DMA), and topped with poly(2-hydroxy ethyl methacrylate) (PHEMA), as flexible surfaces on which fibronectin, an important extracellular matrix component, has been covalently linked. To study the biocompatibility of this type of flexible surface, we coated it with myoblastic cells that can proliferate and then differentiate into myotubes, the constitutive components of muscular fibers. This type of muscular cell has two advantages: first, they grow rapidly, which allows measuring of their well-being on the PET-DMA-PHEMA membranes by counting them along time and quantifying their rate of growth: second, after reaching confluence, muscular cells spontaneously differentiate. The differentiation process is sensitive to the cellular environment, and particularly to the nature of the surface on which cells are growing [36]. We therefore used the capacity of differentiation into myotubes as essential criteria to quantify the quality of flexible surfaces studied in this work.

For this purpose, we have assessed the propensity of muscular cells to grow and differentiate on Fibronectin-coated, PHEMA-modified PET substrates. Herein, we show for the first time that this device combines flexibility as well as a good attachment for eukaryotic cells and enhancement of their proliferation and differentiation.

## 2. Experimental

### 2.1. Materials

2-hydroxyethyl methacrylate (HEMA, 130.14 g/mol, Aldrich, Steinheim, Germany) and poly(ethylene glycol diacrylate) (PEGDA, average 700 g/mol, Aldrich, Steinheim, Germany) were purified by filtering through basic alumina ( $\text{Al}_2\text{O}_3$ ) column to remove the inhibitor, and then stored in the fridge before use. *N,N*-Dimethyl-*p*-phenylenediamine (99.5% purity, Acros, Gelnhausen, Germany), isopentyl nitrite (purity ~97%, Alfa Aesar, Kandel, Germany), 1,1'-carbonyldiimidazole (CDI, Aldrich, Steinheim, Germany), and benzophenone (Aldrich, Steinheim, Germany) were used as received. Solvents including

acetonitrile (ACN), methanol (MeOH), ethanol (EtOH), dimethyl sulphoxide (DMSO), dimethyl formamide (DMF) were purchased from VWR (Fontenay-sous-Bois, France). The organic solvents used were analytical grade and de-ionized water (DI) was used for various cleaning and solution preparation. The PET sheets (thickness ~100  $\mu\text{m}$ ) were purchased from TechNova (Mumbai, India), and cut into sizes of 30  $\times$  15 mm-sized strips.

### 2.2. Functionalization of PET Substrate by Arylation with Diazotized *N,N*-Dimethyl-*p*-phenylenediamine (DMA)

The PET sheets were cleaned and activated prior to diazonium functionalization. First, they were ultrasonically cleaned with chloroform and ethanol for 15 min and then dried with argon flush. Before diazonium functionalization, the PET sheets were hydroxylated in a DMSO solution of potassium hydroxide (4 mg KOH dissolved in 30 mL DMSO; KOH concentration =  $2 \times 10^{-3} \text{ mol}\cdot\text{L}^{-1}$ ) for 10 min maximum, then washed with copious amounts of DI water and dried in argon flow. The surface chemical modification of PET sheets was carried out using the diazonium salt of DMA. Typically, a three necked round bottomed flask (vol: 100 mL) with a reflux condenser arrangement was used for the functionalization reaction. The flask with the colorless, transparent substrate was kept on a preheated oil bath and DMA (15 mmol, 2.04 g) was introduced. Cautiously isopentyl nitrite (15 mmol, 2.01 mL) was added slowly via syringe and 10 mL DMF was also added for solubilization. The reaction was left to proceed for 5 h at 60  $^{\circ}\text{C}$  under continuous argon bubbling. Finally, the yellow colored modified substrates were thoroughly washed with DMF, DI water, and dried under argon flow.

### 2.3. Surface-Confined Photopolymerization

A typical procedure of photopolymerization of HEMA on DMA modified PET surface was as follows. A homogeneous solution of HEMA monomer (20 mmol, 2600 mg) and benzophenone (208 mg, 8% wt percent relative to monomer), as photosensitizer, were prepared in chloroform (20 mL) in a glass bottle. The DMA-modified PET was dipped in the mixture and bubbled with argon gas for 15 min to degas. Radical photopolymerization was carried out using a Spectrolinker XL-1500 equipped with six lamps emitting light nominally at 365 nm with a power density of 5 mW/cm<sup>2</sup>. The photopolymerization time was 1200 s. To study the effect of crosslinker, in the present case, poly-ethylene glycol diacrylate (PEGDA), we have added two different weight percents (1% and 10% with respect to total weight of monomer and crosslinker) of crosslinker with HEMA monomer. The use of crosslinker ensures better adhesion of the photopolymerized top layer to the substrate [37]. The polymerized sample was then taken out of the glass bottle and washed with methanol in a Soxhlet extractor for 2 h to remove the unreacted monomer and then washed with copious amounts of dichloromethane to remove organic species. Finally, the polymer-coated sheets were dried under argon flow and used in the next step of surface modification.

### 2.4. Immobilization of Fibronectin Protein

Before the fibronectin protein immobilization, the polymer coated surface was activated by Imidazolyl carbamate. These moieties were attached to the polymer surface by the reaction of CDI (10 g/L in dioxane) with the hydroxyl group of PHEMA. The reaction was carried out for 6 h at room temperature. Finally, activated surfaces were thoroughly washed with dioxane and phosphate-buffered saline (PBS) solution to remove unreacted CDI. The covalent protein immobilization was performed by immersing the CDI activated surface in a fibronectin protein solution for 25 h under bidirectional stirring. The protein immobilization was tuned by changing the protein concentration ranging from 0.5 to 20  $\mu\text{g}/\text{mL}$ . After the protein attachment the surfaces were carefully rinsed with 5% (*v/v*) aqueous solution of tween20 to remove unattached protein and then finally the surface was cleaned with DI water.

## 2.5. XPS Surface Characterization

Surface chemical analysis was performed using a Thermo VG ESCALAB 250 X-ray photoelectron spectrometer (XPS) fitted with an Al monochromatic X-ray source ( $h\nu = 1486.6$  eV; spot size = 500  $\mu\text{m}$ ). The samples were mounted on the sample holder using double-sided adhesive tapes. Binding energy positions were calibrated against the C-C/C-H C1s peak position set at 285.0 eV. Elemental atomic concentrations were calculated from the XPS peak areas and the corresponding Scofield sensitivity factors corrected for the analyzer transmission work function.

## 2.6. Cell Adhesion

Murine C2C12 myoblastic cells were obtained from the American Type Culture Collection (ATCC<sup>®</sup>, reference CRL-1772<sup>™</sup>), and used between passages 3 and 10.

PET membranes were first sterilized by rinsing with ethanol 70% and then put down in 6-well cell culture dishes. 25,000 C2C12 cells were plated with 2 mL of Dulbecco Modified Eagle Medium (DMEM glutamax, Life Technologies, Illkirch-Graffenstaden, France), supplemented with 10% (or 2%) of bovine calf serum. Observations and photographs were performed on a AxioA1 microscope with a 10 $\times$  objective and an AxioCam camera (Zeiss, Marly le Roi, France).

## 3. Results and Discussion

### 3.1. General Procedure to Modify PET Surface for Cell Adhesion and Growth of Muscle Fibers

Figure 1 displays the steps to the growth of muscular fibers on biocompatible, flexible PET sheets. After activation of PET by KOH, the *N,N*-dimethylaminobenzenediazonium cation was generated in situ and reacted with the activated PET. The PET sheet turned to yellow and remained transparent; it is defined as PET-DMA and served as macro-hydrogen donor in the photopolymerization process. Then HEMA was photopolymerized or copolymerized with PEGDA using benzophenone as photosensitizer to yield PHEMA or crosslinked PHEMA films on PET (PET-DMA-PHEMA or PET-DEMA-PHEMA/PEGDA) which were further activated by CDI to obtain imidazole-functionalized PHEMA grafts for the attachment of fibronectin. The final fibronectin-functionalized plate (PET-DMA-PHEMA-I-FBN) served for eukaryotic cell adhesion and growth of muscular fibers.

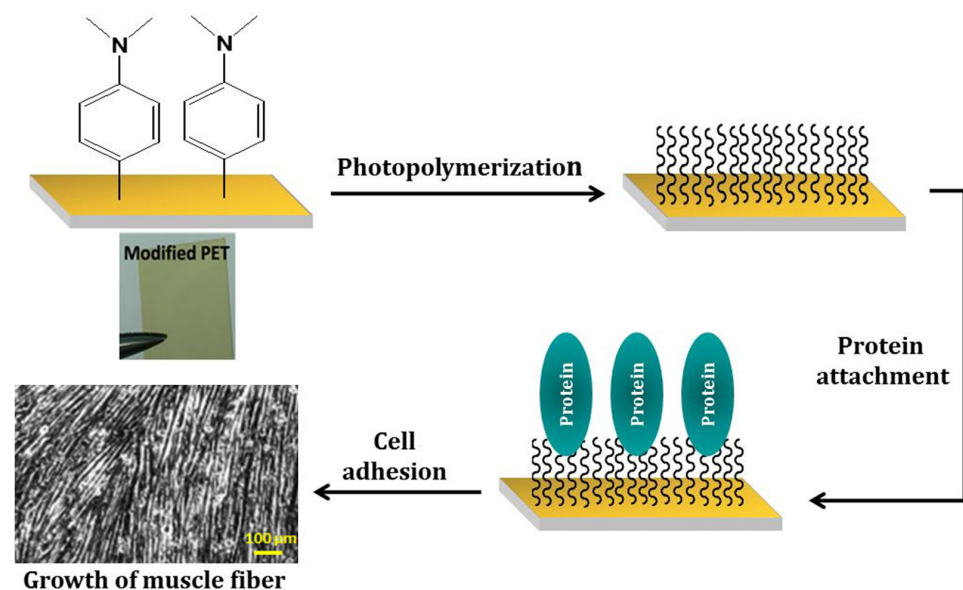


**Figure 1.** Sequential steps of the growth of muscle fibers onto flexible, bioactive PET sheets. Upper panel: diazonium modification of PET for the grafting of radical photoinitiator and PET surface-confined photopolymerization process for grafting PHEMA or PHEMA/PEGDA nanofilms. Lower panel: immobilization of fibronectin followed by cell adhesion and growth of muscular fibers.

### 3.2. Surface Characterization of PET Surfaces by XPS

#### 3.2.1. Survey Regions and Surface Elemental Composition

Typical survey regions for selected clean and coated PET sheets are displayed in Figure 2. Qualitatively, it is worth noting the efficiency of each step towards the preparation of bioactive platforms for cell adhesion. The main peaks C1s, O1s, and N1s are centered at 285, 532, and 400 eV, respectively. The activated, clean PET displays only C1s and O1s peaks (Figure 2a) while the diazonium attachment is testified by the appearance of an N1s peak from the grafted DMA aryl groups (Figure S1a). With an initial concentration of the photosensitizer benzophenone of 8% (benzophenone to monomer molar ratio) it was possible to graft a PHEMA top layer, thick enough (well above 10–12 nm) to screen the underlying DMA aryl layer. For this reason, the N1s peak is no longer visible on the survey scan (Figure 2b). However, after activation of polymer OH groups by CDI, hydroxyl groups convert to carbamates, hence the appearance of the N1s peak again (Figure S1b). Immobilization of fibronectin was tuned by changing the initial concentration of fibronectin from 0.5 to 20  $\mu\text{g}/\text{mL}$ .

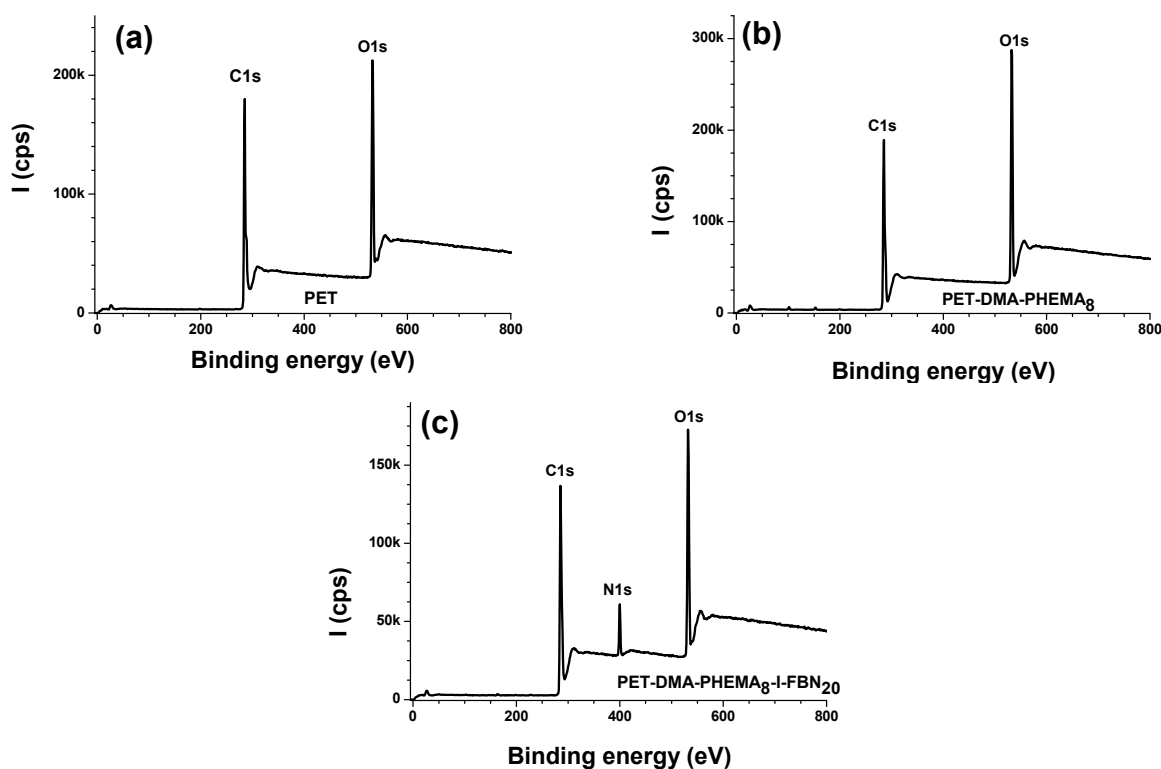


**Figure 2.** Survey regions of bare and modified PET. (a) PET, (b) PET-DMA-PHEMA<sub>8</sub>, (c) PET-DMA-PHEMA<sub>8</sub>-I-FBN<sub>20</sub>.

Figure 2c shows that the relative intensity of the N1s peak is significantly higher than that exhibited by PET-PHEMA-FBN<sub>2</sub> (Figure S1c). The survey spectra permit thus to qualitatively monitor the sequential changes occurring at the surface, simply by tracking the relative intensity of the N1s peak.

Table 1 reports the surface chemical composition (in at. %) of bare and modified PET sheets.

**Table 1.** Surface chemical composition (in at. %) of bare and modified PET sheets.

Materials	% C	% O	% N	% S
PET (KOH-activated)	74.4	25.6	0	-
PET-DMA	71.7	25.1	3.3	-
PET-DMA-PHEMA	71.8	28.0	0.2	-
PET-DMA-PHEMA-I	50.7	46.7	2.6	-
PET-DMA-PHEMA-I-FBN <sub>0.5</sub>	70.9	27.0	2.1	traces
PET-DMA-PHEMA-I-FBN <sub>2</sub>	70.2	28.0	1.7	0.1
PET-DMA-PHEMA-I-FBN <sub>5</sub>	69.8	26.8	3.3	0.1
PET-DMA-PHEMA-I-FBN <sub>10</sub>	69.6	25.2	5.0	0.2
PET-DMA-PHEMA-I-FBN <sub>20</sub>	68.5	24.3	7.0	0.2
PET-DMA-PHEMA-PEGDA <sub>1</sub>	69.3	30.4	0.3	-
PET-DMA-PHEMA-PEGDA <sub>10</sub>	69.3	30.5	0.2	-
PET-DMA-PHEMA-PEGDA <sub>1</sub> -I	49.2	48.7	2.2	-
PET-DMA-PHEMA-PEGDA <sub>10</sub> -I	46.5	53.2	0.3	-
PET-DMA-PHEMA-PEGDA <sub>1</sub> -I-FBN <sub>20</sub>	49.8	49.1	1.0	~0.1
PET-DMA-PHEMA-PEGDA <sub>10</sub> -I-FBN <sub>20</sub>	49.5	49.6	0.8	~0.1

### 3.2.2. High Resolution Regions

#### C1s

Figure 3 displays the high resolution C1s spectra of PET, PET-DMA, PET-DMA-PHEMA, and PET-DMA-PHEMA-I-FBN<sub>20</sub>. PET C1s peak is fitted with 4 components centered at 285.0, 286.5, 289.0, and 291.5 assigned to C-C/CH,  $\underline{\text{C}}\text{H}_2\text{-O}$ ,  $\text{O-}\underline{\text{C}}=\text{O}$ , and the shake-up satellite, respectively (Figure 3a). After DMA attachment to PET, the component at 286.4 eV has a higher contribution due to the C-N bonds in the aryl layer (Figure 3b). Similarly, the shake-up satellite contribution is increased due to the attachment of the aryl layer. Photopolymerization of HEMA induces a drastic change in the C1s structure: the peak is fitted with 3 components centered at 285.0, 286.6, 288.9 eV; and the shake-up satellite is suppressed as the PET is very well screened (Figure 3c). The activation of the OH groups by CDI induces slight changes in the shape of the C1s region. Finally, the covalent attachment of fibronectin induces the appearance of a peak at 287.7 eV due to the amide groups from the protein (Figure 3d). One can also note a component centered at 290.7 eV due to polymer–fibronectin interfacial carbamate group (N-COO). As all proteins have a prominent peak at 286–286.5 eV, it follows that fibronectin induces an increase in the contribution of the peak centered at 286.4 eV to the total C1s region (Figure 3d). The contribution of the amide N-C=O groups (specific of peptidic linkage) to the C1s peak area is plotted against the initial concentration of fibronectin (in  $\mu\text{g}/\text{mL}$ ). One can see that a steady state is reached for an initial concentration of  $\sim 10 \mu\text{g}/\text{mL}$  (Figure 3e).

#### O1s

The main information that can be obtained from O1s regions is the change from PET to a PHEMA-rich surface (Figure S2). PET has two ester groups per repeat unit and thus one carbonyl and one alkoxy groups which are known to give a well resolved doublet as displayed in Figure S2a. After photopolymerization and the build-up of a quite thick PHEMA layer, one obtains a broad O1s peak fitted with three components assigned to the carbonyl, OH, and the ethoxy groups of HEMA repeat units (Figure S2b). It follows that the O1s regions testify to the drastic change from PET to PHEMA after surface-confined radical photopolymerization.

#### N1s and S2p

Figure S3 displays selected high resolution N1s regions from PET-DMA, PET-DMA-PHEMA-I, and PET-DMA-PHEMA-I-FBN<sub>5</sub>: the N1s from PET-DMA (Figure S3a) has two contributions assigned to the free dimethylamino groups (main component) at 399.2 eV and the azo groups at  $\sim 401$  eV included in the polyphenylene-like chain. Figure S3b displays an N1s peak from PET-DMA-PHEMA-I assigned to the attached imidazole group.

Upon covalent binding of fibronectin, one can see that the N1s peak has a high signal to noise ratio, centered at  $\sim 400$  eV (Figure S3c) and assigned to the peptidic links in the attached protein.

Figure S4 displays the S2p narrow regions from the fibronectin-topped sheets prepared with 0.5 and 5% initial fibronectin concentration. Obviously, one switches from a noisy, flat background to an S2p signal that rises above the baseline. Sulfur from the top layer gives noisy peaks; it is nevertheless an important element to track at the surface as it is a unique marker for fibronectin. S2p gives thus strong supporting evidence for the attachment of fibronectin and firmly confirms the success of the final surface chemical reaction we have performed on the flexible plastic sheets.

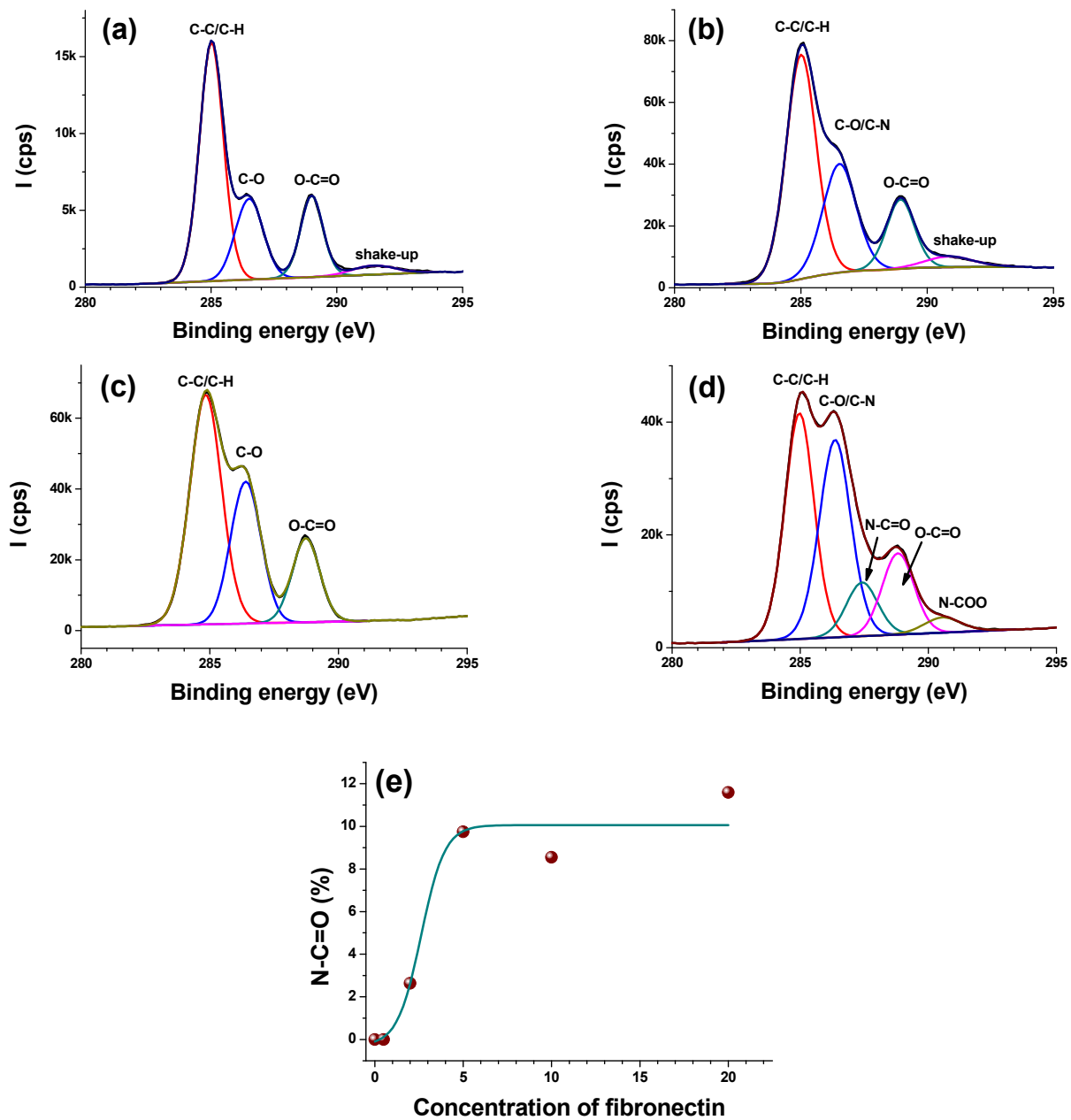


**Figure 3.** High resolution C1s regions from (a) PET, (b) PET-DMA, (c) PET-DMA-PHEMA, and (d) PET-DMA-PHEMA-I-FBN<sub>5</sub>. (e) The contribution of N-C=O (amide) groups to the C1s peak is plotted versus fibronectin concentration (in %).

### 3.3. Cell Adhesion and Growth of Muscular Fibers

Cell growth and differentiation require a biocompatible surface and optimal environmental parameters. For this reason, flexible PET surfaces were first grafted with PHEMA and further functionalized with fibronectin. The as-modified PET sheets were employed as bioactive platforms for the attachment of myoblastic cells. Hereafter, we investigate the propensity of the cells to proliferate and differentiate into myotubes on the bioactive PET sheets.

We thus first investigated how eukaryotic C2C12 cells attach and grow on various PET surfaces. These surfaces were treated as described above (abbreviated as PET-DMA-PHEMA-I). To better understand how these surface treatments modulate cell growth, we used PET-DMA-PHEMA-I membranes on which fibronectin was covalently attached. The rationale for topping the PHEMA-grafted PET sheets with fibronectin is that this protein is a natural component of the extracellular matrix known to favor growth and differentiation of cells [20]. Fibronectin was grafted on PET-DMA-PHEMA-I using an initial concentration of 5, 10 or 20  $\mu\text{g}/\text{mL}$ . The resulting bioactive platforms are abbreviated PET-DMA-PHEMA-I-FBN<sub>x</sub>,  $x = 0.5, 2, 5, 10,$  and  $20 \mu\text{g}/\text{mL}$ . Control substrates were PET membranes without any treatment (PET), untreated PET sheets incubated with 5  $\mu\text{g}/\text{mL}$  fibronectin (PET-FBN<sub>5</sub>), and grafted PET membranes without CDI but coated with fibronectin (PET-DMA-PHEMA-FBN<sub>20</sub>). In addition, a glass coverslip (GCS) was incubated with 5  $\mu\text{g}/\text{mL}$  fibronectin, which is usually used in biological studies for cell growth and differentiation (GCS-FBN<sub>5</sub>).

Prior to cell growth, the samples were cut to 1  $\text{cm}^2$  and placed at the bottom of one well (5.5  $\text{cm}^2$ ) in a 6-well plastic culture dish. In each well, 25,000 murine myoblastic cells were plated in the growth medium, and left to grow for a set period of time. The number of cells present in 5 fields (0.6  $\text{mm}^2$ ) taken randomly on the PET surfaces were counted daily. Figure 4 displays the mean value of the number of cells on the PET surface versus elapsed time from the start of plating. Cell growth was quantified by fitting the plots to exponentials, and the exponential coefficient  $k$  was calculated (Table 2). The decreasing trend of cell growth is PET-DMA-PHEMA-I-FBN<sub>20</sub> ( $k = 0.35 \text{ d}^{-1}$ ) > PET-DMA-PHEMA-I-FBN<sub>10</sub> ( $k = 0.27 \text{ d}^{-1}$ ) > PET-DMA-PHEMA-I-FBN<sub>5</sub> ( $k = 0.24 \text{ d}^{-1}$ ) > PET ~ PET-FBN<sub>5</sub> ( $k = 0.23 \text{ d}^{-1}$ ) > and then PET-DMA-PHEMA-FBN<sub>20</sub> ( $0.21 \text{ d}^{-1}$ ), which indicates that control surfaces are less efficient than fully grafted fibronectin-PET membranes. Finally, the “usual” glass coverslip coated with fibronectin, GCS-FBN<sub>5</sub>, displayed the lowest growth rate  $k = 0.17 \text{ d}^{-1}$ . Clearly, grafting flexible PET surfaces with fibronectin yields two-fold growth rate in comparison to “classical” fibronectin-coated glass surface currently used by biologists, and anticipates interesting uses for these types of surfaces in the future.

**Table 2.** Measurement of cell growth on glass and PET surfaces. Curves of cell growth were fitted to exponential curves, and the exponential coefficient  $k$ , which indicates the speed of growth (in  $A = A_0 e^{kt}$ ) calculated. Another way to estimate cell growth is the doubling time (half-time) calculated (half-time =  $\ln(2)/k$ ) and shown in the right column.

PET Surfaces	Exponential Coefficient ( $k$ )	Half-Time (Days)	Figure
GCS-FBN <sub>5</sub>	0.17	4.1	4
PET	0.23	3.0	4
PET-FBN <sub>5</sub>	0.23	3.0	4
PET-DMA-PHEMA-FBN <sub>20</sub>	0.21	3.3	4
PET-DMA-PHEMA-I-FBN <sub>5</sub>	0.24	2.9	4
PET-DMA-PHEMA-I-FBN <sub>10</sub>	0.27	2.6	4
PET-DMA-PHEMA-I-FBN <sub>20</sub>	0.35	2.0	4
PET	0.24	2.9	5
PET-DMA-PHEMA	0.20	3.5	5

Table 2. Cont.

PET Surfaces	Exponential Coefficient ( $k$ )	Half-Time (Days)	Figure
PET-DMA-PHEMA-PEGDA <sub>1</sub>	0.38	1.8	5
PET-DMA-PHEMA-PEGDA <sub>10</sub>	0.38	1.8	5
PET-DMA-PHEMA-PEGDA <sub>1</sub> -I-FBN <sub>20</sub>	0.44	1.6	5
PET-DMA-PHEMA-PEGDA <sub>10</sub> -I-FBN <sub>20</sub>	0.42	1.7	5

In order to improve the chemical treatment of the PET surfaces, we modified the protocol of radical photopolymerization of HEMA on PET-DMA by adding PEGDA comonomer at 1% or 10% relative to HEMA. HEMA and PEGDA were co-photopolymerized in order to obtain crosslinked, biocompatible polymer grafts with improved polymer adhesion to diazonium-modified surfaces [37]. Investigations of cell growth were conducted in a similar manner as described above in Figure 4. Results are presented in Figure 5 and Table 2. The half-time defined as  $\ln(2)/k$  is another way to measure cell growth; the lowest values (in days) correspond to the most favorable surfaces, whereas the highest values indicate less favorable surfaces for cell growth. As far as the  $k$  values are concerned, Table 2 shows that cell growth on PET-DMA-PHEMA-PEGDA<sub>x</sub>-I-FBN<sub>20</sub> ( $x = 1$  and 10%) reached an exponential coefficient  $k$  of 0.44 and 0.42  $\text{d}^{-1}$ , and was higher than PET-DMA-PHEMA-FBN<sub>20</sub> ( $k = 0.35 \text{ d}^{-1}$ ) displayed in Figure 4. This rate of growth was 10 to 15% higher than for PET-DMA-PHEMA-PEGDA<sub>x</sub>-I sheets but without any addition of fibronectin (0.38  $\text{d}^{-1}$ ). Interestingly, treatment with PEGDA considerably improves cells growth on this surface without fibronectin (PET-DMA-PHEMA-PEGDA<sub>x</sub>-I,  $k = 0.38 \text{ d}^{-1}$ ), by almost 100% compared to PET-DMA-PHEMA ( $k = 0.20 \text{ d}^{-1}$ ), a platform that bears neither PEGDA nor fibronectin. Altogether, these results suggest that treatment with PEGDA considerably improves the efficiency of cell growth (on PET-DMA-PHEMA-PEGDA<sub>x</sub>-I-FBN surfaces).

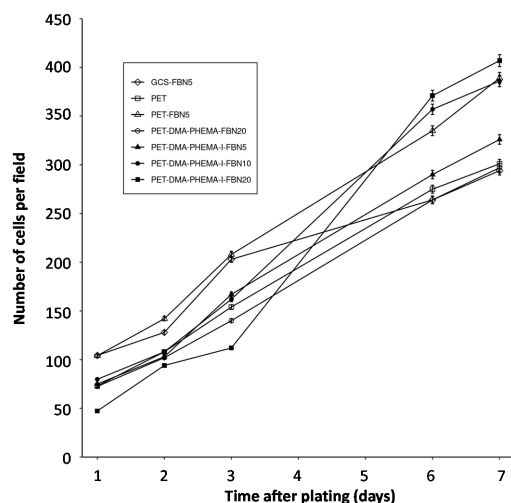


**Figure 4.** Cell growth on PET membranes. C2C12 myoblastic cells were plated on plastic dishes containing PET substrates subjected to various treatments. The day of plating was defined as day 0. Cells were grown on regular medium supplemented with calf serum and antibiotics. At days 1, 2, 3, 6, and 7 after plating, 5 fields taken at random above PET substrates were visualized under microscope and the number of cells counted. GCS-FBN<sub>5</sub>: glass coverslips coated with 5  $\mu\text{g}/\text{mL}$  of fibronectin, PET: untreated PET sheets, PET-FBN<sub>5</sub>: untreated PET membranes coated with 5  $\mu\text{g}/\text{mL}$  of fibronectin, PET-DMA-PHEMA-FBN<sub>20</sub>: PET membranes grafted but not treated with CDI, and then coated with 20  $\mu\text{g}/\text{mL}$  of fibronectin, PET-DMA-PHEMA-I-FBN<sub>x</sub>: PET membranes grafted with the DMA, PHEMA, imidazole and reacted with fibronectin at initial concentration  $x = 5, 10$ , and 20  $\mu\text{g}/\text{mL}$  respectively.

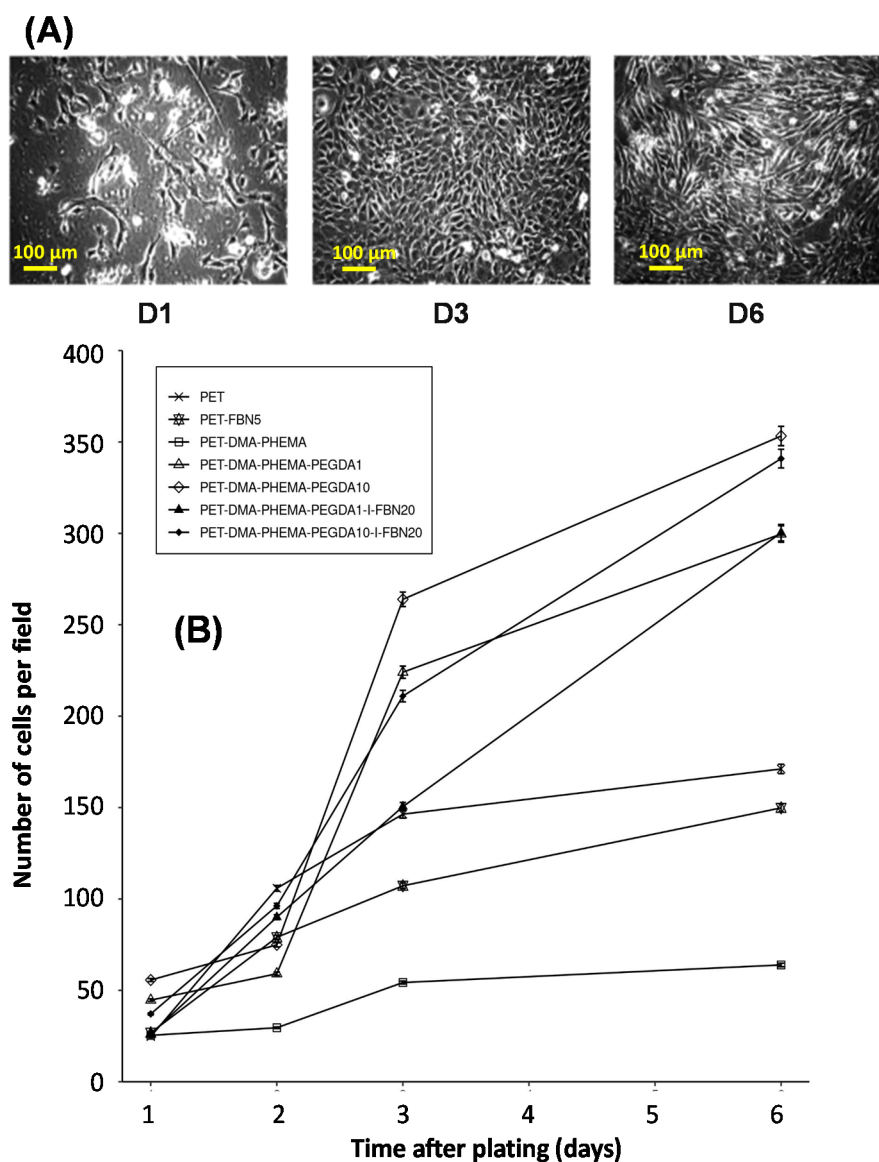


**Figure 5.** Cell growth on PET membranes treated with PEGDA. **(A)** Photomicrographs displaying cell growth on PET-DMA-PHEMA-PEGDA<sub>10</sub>-I-FBN<sub>20</sub> membranes at day 1 (D1), 3 (D3), and 6 (D6) after plating. Please note the considerable densification of cells on the surface. **(B)** C2C12 myoblastic cells were plated on plastic dishes containing PET membranes grafted with PEGDA the day 0. The graph reports the number of cells counted in 5 independent fields taken randomly on the PET sheets, at different days following plating. PET: untreated PET sheets, PET-FBN<sub>5</sub>: untreated PET membranes coated with 5 μg/mL of fibronectin, PET-DMA-PHEMA: PET membranes stopped at the PHEMA grafting step, PET-DMA-PHEMA-PEGDA<sub>1</sub> and PET-DMA-PHEMA-PEGDA<sub>10</sub>: PEGDA-containing PET prepared using 1% and 10% PEGDA relative to HEMA, respectively, PET-DMA-PHEMA-PEGDA<sub>x</sub>-I-FBN<sub>20</sub>: PET sheets grafted with crosslinked copolymers of HEMA and PEGDA using 1% and 10% PEGDA (relative to HEMA) and finally grafted with 20 μg/mL of fibronectin after imidazole activation.

A second important biological parameter to investigate is the capacity of the cells to differentiate; it indicates how cells adequately interact with the support on which they grow. Indeed, it is well known that differentiation is obtained only if cellular environmental parameters are optimal with regard to reduced growth factors in culture medium as well as attachment to extracellular molecules such as fibronectin. For that purpose, all myoblast cells were left to grow to confluence without changing the culture medium after day 7, and

thus to allow exhaustion of growth factors. In these conditions, cells switch from a growth program to a differentiation program: they align in a parallel fashion and start to fuse together to give multinucleated myotubes (Figure 6A). At this step, cell culture medium is renewed, but the fetal calf serum providing growth factors is reduced to 2% instead of 10% to allow cell survival but not cell growth. To quantify cell differentiation, the number and diameter of the myotubes adhering to the PET surfaces were determined.

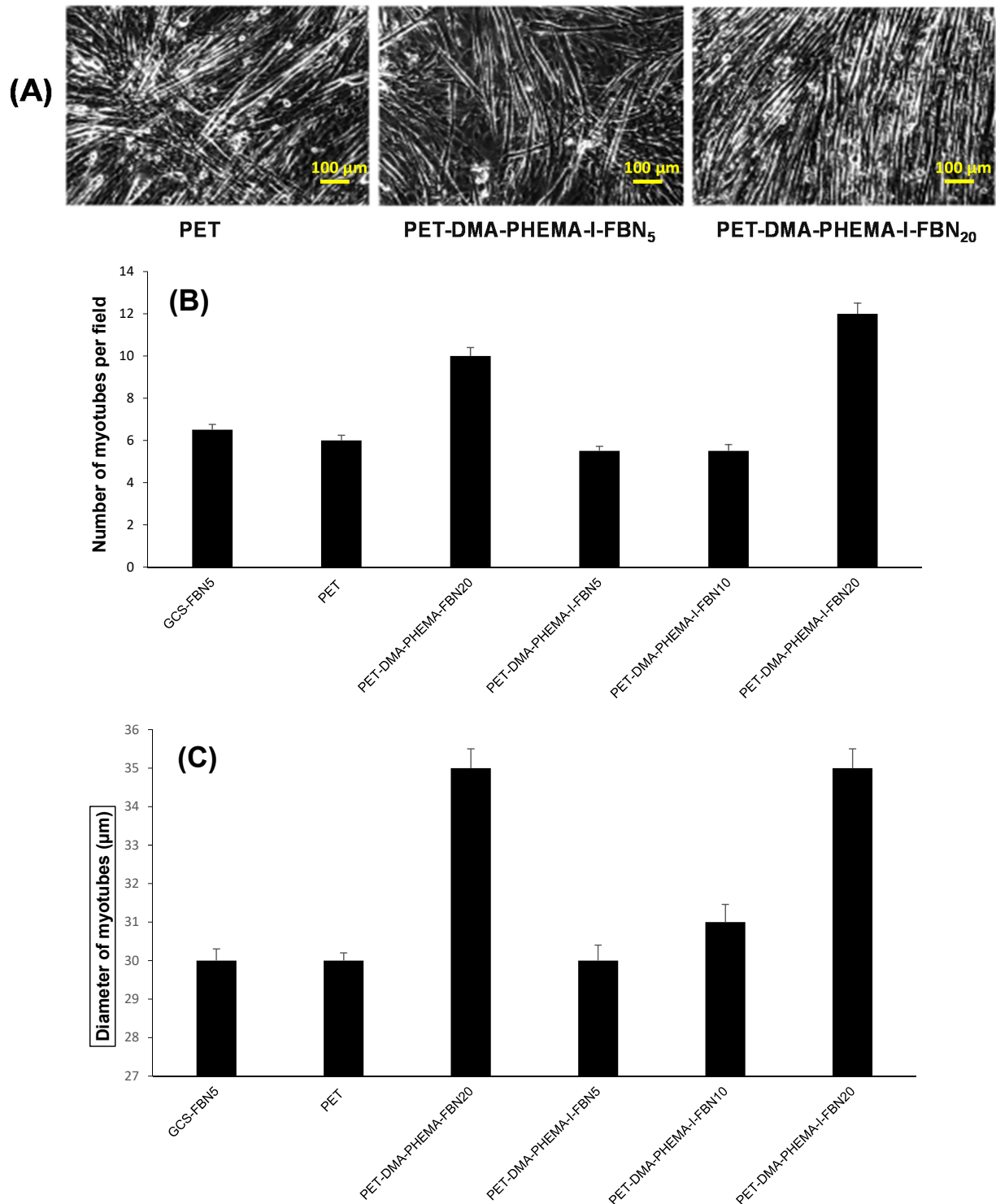


**Figure 6.** Cell differentiation on PET membranes. (A) Photomicrographs representative of cell differentiation on PET membranes. Photographs were taken at day 7 after plating, for PET, PET 5 FBN, and PET 20 FBN membranes. Fusiform long

structures are differentiated myotubes resulting from the fusion of individual myoblasts. **(B)** Number of myotubes. C2C12 muscular cells were plated at day one at the same conditions as for Figure 4. They were left 7 days to grow and differentiate. At day 7 the medium was changed from growth medium to differentiation medium. Differentiation was characterized by cell fusion into long multinucleated myotubes. At day 7, the number of myotubes on PET membranes was counted on 5 different fields. The mean value of the number of myotubes is shown on PET surfaces subjected to various treatments. **(C)** Diameter of myotubes. Photographs of the fields were taken and the diameter of myotubes measured. The average value is reported on the graph, depending on the various treatment of PET supports. Glass + FBN: glass coverslips coated with 5  $\mu\text{g}/\text{mL}$  of fibronectin. PET NT: untreated PET membranes. PET NT 5 FBN: untreated PET membranes coated with 5  $\mu\text{g}/\text{mL}$  of fibronectin. PET PHEMA 20 FBN: PET membranes grafted but not treated with CDI, and coated then with 5  $\mu\text{g}/\text{mL}$  of fibronectin. PET-DMA-PHEMA-I-FBN<sub>5</sub>, PET-DMA-PHEMA-I-FBN<sub>10</sub>, PET-DMA-PHEMA-I-FBN<sub>20</sub>: PET membranes grafted with DMA-PHEMA-I and then with fibronectin at 5, 10 and 20  $\mu\text{g}/\text{mL}$ , respectively.

Differentiation was assessed on PET-DMA-PHEMA-I-FBN<sub>x</sub> ( $x = 5, 10$  and  $20 \mu\text{g}/\text{mL}$  of fibronectin), with the same conditions as used for Figure 4. After 8 days of cell plating, myotubes were already well developed, with a density between 6 and 12 per  $0.6 \text{ mm}^2$  field (see Figure 6A). The best result is obtained with PET-DMA-PHEMA-I-FBN<sub>20</sub> (12 myotubes per field), while lower concentrations (5 and 10  $\mu\text{g}/\text{mL}$  fibronectin) remained at basal levels, equivalent to untreated PET surfaces (PET) that is 6 myotubes per field (Figure 6B).

Interestingly, PET-DMA-PHEMA-FBN<sub>20</sub> gives also a high level of differentiation, with 10 myotubes per field, slightly lower than PET-DMA-PHEMA-I-FBN<sub>20</sub>. In these conditions, fibronectin is adsorbed on the surface, but without any covalent bonding. Similar results were obtained after 10 and 13 days of culture and differentiation (data not shown).

The number of myotubes shown in Figure 6B does not take into account the evolution of differentiation once the myotubes are formed: when two cells fuse together, it is already considered as a myotube, but differentiation still goes on and other myoblasts fuse to this myotube, allowing it to grow in length, diameter, and number of nuclei. Therefore, in order to better quantify the progression of differentiation, the diameter of myotubes was measured. Indeed, the diameter is proportional to the number of cells that have fused into myotubes. Results are shown in Figure 6C, and are essentially similar to those displayed in Figure 6B: the diameter of myotubes reaches 35  $\mu\text{m}$  with 20  $\mu\text{g}/\text{mL}$  FBN grafted to the PET surface (PET-DMA-PHEMA-I-FBN<sub>20</sub>), equivalent to the control PET-DMA-PHEMA-FBN<sub>20</sub>. PET-DMA-PHEMA-I-FBN<sub>5</sub> was equivalent to the untreated, bare PET surface with a diameter of 30  $\mu\text{m}$ . It should be noted that this parameter shows less variation from 30 to 35  $\mu\text{m}$  of myotube diameter (maximum  $\sim 20\%$  variation) than changes in the number of myotubes per field (from 6 to 12) when surfaces are differently treated. This result suggests that it is less difficult for cells to form a new myotube than to fuse and grow in diameter of the already created myotubes.

In addition, and as shown in Figure 5, we used conditions of preparation and grafting PET surfaces for myoblastic differentiation with addition of PEGDA crosslinker for PHEMA. Figure 7A shows that after 8 days of growth and differentiation, myotubes differentiated on PET with 10% PEGDA and 20  $\mu\text{g}/\text{mL}$  of fibronectin (PET-DMA-PHEMA-PEGDA<sub>10</sub>-I-FBN<sub>20</sub>) are present at the highest number (left panel), compared to 10% PEGDA without fibronectin (PET-DMA-PHEMA-PEGDA<sub>10</sub>), at a level equivalent to the control PET-DMA-PHEMA. Quantification of the mean number of myotubes per field (Figure 7B) shows that after 8 days of growth and differentiation, PET-DMA-PHEMA-PEGDA<sub>10</sub>-I-FBN<sub>20</sub> gives the highest number of myotubes, followed by PET-DMA-PHEMA-PEGDA<sub>1</sub>-I-FBN<sub>20</sub>, at a level equivalent to the control PET-FBN<sub>5</sub>. When PEGDA (1% or 10%) is added, but not FBN, the number of myotubes per field is reduced to a number similar to the control PET. Therefore, these results clearly indicate that addition of PEGDA potentiates the effect of FBN. Thus, treatment with PEGDA, even at a low concentration of 1% may potentiate the efficiency of the PET membranes for myoblasts differentiation.

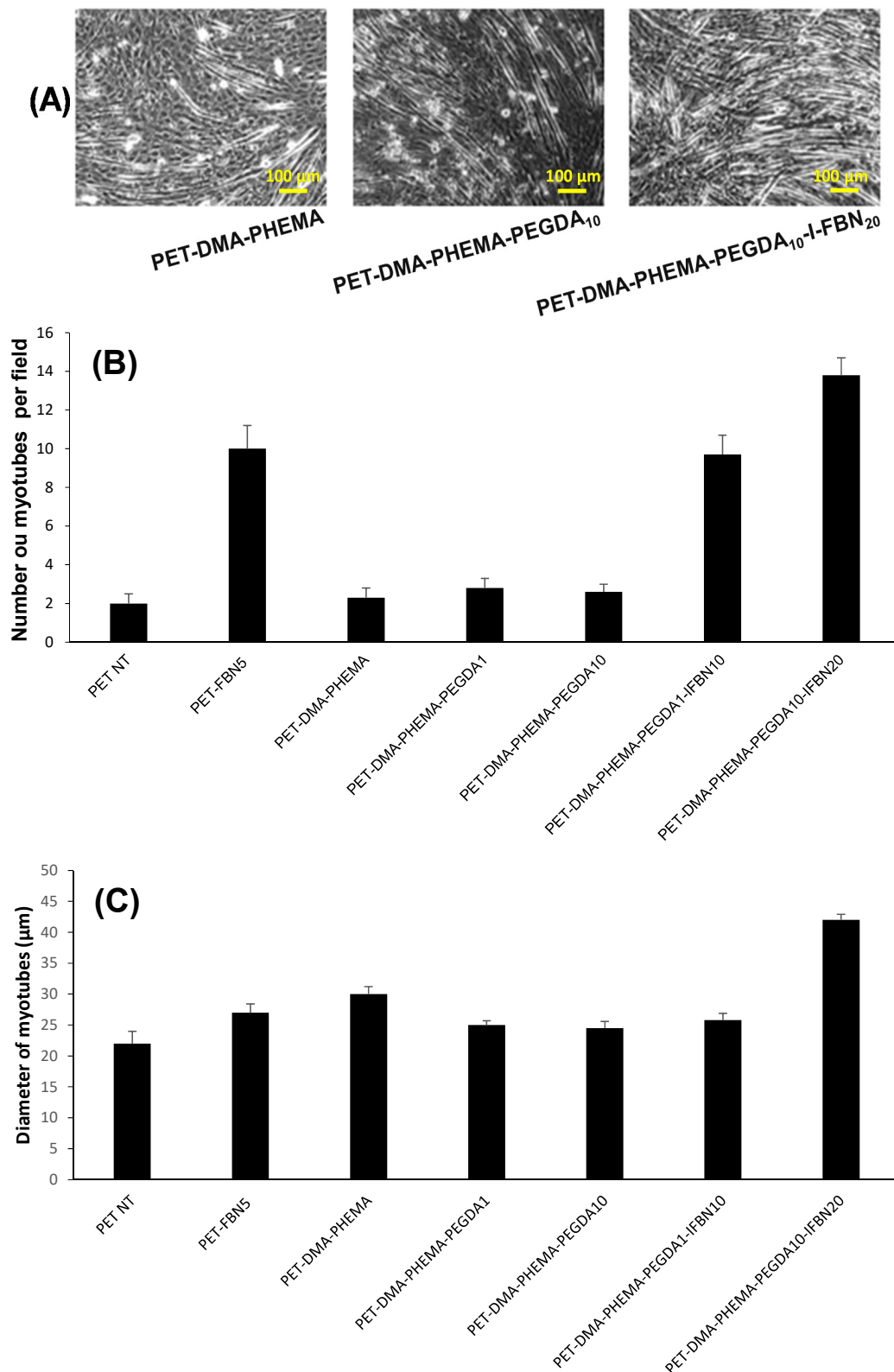


**Figure 7.** Cell differentiation on PET membranes treated with PEGDA. C2C12 muscular cells were plated at day 0 at the same conditions as for Figure 5. They were left 7 days to grow and differentiate. At day 7, the medium was changed from growth medium to differentiation medium. **(A)** Photomicrographs showing myotubes, the long fusiform multinucleated cells resulting from fusion of individual myoblastic cells, taken 7 days after plating. In the figure, myotubes differentiated on PET-DMA-PHEMA, PET-DMA-PHEMA-PEGDA<sub>10</sub> control membranes, and processed completely with PET-DMA-PHEMA-PEGDA<sub>10</sub>-I-FBN<sub>20</sub> surfaces, are shown. **(B)** At day 8, the number of myotubes on PET membranes was counted on 5 different

fields. The mean value of the number of myotubes is shown on PET surfaces subjected to various treatments. (C) Photographs of the fields were taken and the diameter of myotubes measured. The average value is reported on the graph, depending on the various treatment of PET supports. PET-FBN<sub>5</sub>: untreated PET membranes coated with 5 µg/mL of fibronectin. PET-DMA-PHEM: PET membranes for which the grafting process was stopped at the PHEMA step. PET-DMA-PHEMA-PEGDA<sub>1</sub>, PET-DMA-PHEMA-PEGDA<sub>10</sub>: PET membranes grafted and treated with 1% and 10% PEGDA respectively. PET-DMA-PHEMA-PEGDA<sub>1</sub>-I-FBN<sub>20</sub>, PET-DMA-PHEMA-PEGDA<sub>10</sub>-I-FBN<sub>20</sub>: PET membranes grafted and treated with 1% and 10% PEGDA, respectively, and finally linked to 20 µg/mL of fibronectin.

With regard to myotube diameter (Figure 7C), only the combination of 10% PEGDA and 20 µg/mL of fibronectin (PET-DMA-PHEMA-PEGDA<sub>10</sub>-I-FBN<sub>20</sub>) shows a significantly higher result (45 µm) compared to all other conditions (PET-DMA-PHEMA) at 30 µm of diameter, PET-DMA-PHEMA-PEGDA<sub>1</sub>, PET-DMA-PHEMA-PEGDA<sub>10</sub>, and PET-DMA-PHEMA-PEGDA<sub>1</sub>-I-FBN<sub>20</sub> at 25 µm.

In conclusion, the results obtained so far show altogether that PET membranes grafted with fibronectin at the highest dose (20 µg/mL) through the DMA-PHEMA-I protocol, with addition of PEGDA, is very efficient in allowing proliferation and differentiation of muscular cells.

#### 4. Discussion

Fibronectin, an important component of the extracellular matrix, was grafted on bioactive PET-DMA-PHEMA-I and derivatives in order to investigate proliferation and differentiation of muscular cells on these biomaterials. The general observation is that this type of treatment improves both proliferation and differentiation over untreated or partially treated PET surfaces. Several conclusions can be reached: (i) The untreated PET membrane (Figure 4 and Table 2,  $k = 0.23 \text{ d}^{-1}$ ) provides an improvement of growth over glass slides used in biology (GCS-FBN<sub>5</sub>,  $k = 0.17 \text{ d}^{-1}$ ); (ii) In contrast, PHEMA surfaces (PET-DMA-PHEMA platform), without any post-modification with CDI and fibronectin ( $k = 0.2 \text{ d}^{-1}$ ), might be slightly less efficient for a cell to attach and/or proliferate, compared to PET or PET-FBN<sub>5</sub> ( $k = 0.23 \text{ d}^{-1}$ ), most probably because PHEMA resists protein adsorption and cell adhesion [38]; (iii) When the process of chemical grafting is stopped after the PHEMA step, with no CDI treatment (PET-DMA-PHEMA,  $k = 0.20 \text{ d}^{-1}$ ), addition of fibronectin at high dose does not improve the rate of cell proliferation (PET-DMA-PHEMA-FBN<sub>20</sub>,  $k = 0.21 \text{ d}^{-1}$ ); (iv) this indicates that the post modification by CDI is essential for the efficient covalent attachment of fibronectin; (v) the addition of PEGDA (1% or 10% relative to HEMA co-monomer) on chemically treated surfaces but without any grafted fibronectin markedly enhances the rate of cell division up to  $0.38 \text{ d}^{-1}$ . In addition, this effect is strong enough so that fibronectin grafting then only marginally stimulates the rate of proliferation by 10 to 15%, up to  $0.44 \text{ d}^{-1}$  (PET-DMA-PHEMA-PEGDA<sub>1</sub>-I-FBN<sub>20</sub>). When compared to PET-DMA-PHEMA-I-FBN<sub>20</sub> ( $k = 0.35 \text{ d}^{-1}$ ), addition of PEGDA has a 30% effect and stimulates cell division. The effect of PEGDA could be ascribed to an enhanced biocompatible character imparted by the crosslinker as it is a PEGylated comonomer with an average number 13 of ethylene glycol repeat units per monomer (i.e., per PEGDA). Moreover, polyethylene glycol (PEG) is known to facilitate cell fusion [39].

With regard to cell differentiation, the situation appears more drastic: only the highest dose of fibronectin with PEGDA treatment (PET-DMA-PHEMA-PEGDA<sub>10</sub>-I-FBN<sub>20</sub>, Figure 7A) gives the best number of myotubes, as well as the largest diameter of myotubes, two criteria used to evaluate differentiation. The second best result is provided by PET-DMA-PHEMA-I-FBN<sub>20</sub> (Figure 6A). It appears that fibronectin is essential for a good differentiation, since only PET membranes grafted with fibronectin provide the best results, in number as well in diameter of myotubes (see results in Figures 6 and 7 for PET-DMA-PHEMA-I-FBN<sub>20</sub> and PET-DMA-PHEMA-PEGDA<sub>10</sub>-I-FBN<sub>20</sub>). However, in contrast to results obtained for cell proliferation, PEGDA treatment does not improve differentiation over PET PHEMA (Figure 7A). This result may indicate that if addition of PEGDA stimulates the initial step of differentiation, full differentiation may be obtained

only with the PET 10% PEGDA + 20  $\mu\text{g}/\text{mL}$  of FBN. Altogether, these results suggest that either a threshold concentration of FBN is required for cells to fully differentiate, or that PET-DMA-PHEMA-I may inhibit cell differentiation, by providing inappropriate charges or signals to differentiating cells. This inhibition effect may be overcome by fibronectin when high concentration (20  $\mu\text{g}/\text{mL}$ ) is used. However, these two explanations are not necessarily, mutually exclusive.

The diameter of myotubes may result from a complex situation: when muscular cells reach confluence, they may create with their neighboring cells a new myotube, or fuse with a preexisting myotube. It is possible that chemical treatment of PET membrane modifies this mechanism in a subtle fashion. The main result from this study is that fibronectin is important (PET-DMA-PHEMA-FBN<sub>20</sub> and PET-DMA-PHEMA-I-FBN<sub>20</sub>, Figure 6B) but PEGDA improves the diameter, although PET-DMA-PHEMA gives a slightly higher value (Figure 7B) possibly due to improved biocompatibility imparted by PHEMA. In order to have a complete picture, it would be interesting to investigate the roughness of the substrate as this physical parameter might influence cell adhesion [40].

## 5. Conclusions

To sum up, we have modified transparent, flexible, biaxially oriented polyethylene terephthalate (PET) sheets with bioactive polymer–fibronectin top layers via a stepwise surface chemical procedure. After activation by KOH, PET was modified with diazonium salts in order to have a surface able to initiate radical photopolymerization of HEMA resulting in robust, covalently grafted PHEMA, or crosslinked PHEMA if the photopolymerization was conducted in the presence of the crosslinker EGDA. The biocompatible thin polymer top layer was further activated with carbonyl diimidazole in view of covalently attaching fibronectin (FBN). All modification steps were validated by high resolution XPS analysis. The resulting FBN-conjugated thin polymer layers served for the attachment of cells and growth of muscle fibers. We found that the full treatment, with PEGDA and fibronectin, gave the best results in all cases, and stimulates cell proliferation as well as differentiation and growth of myotubes. This opens avenues for providing favorable environments for cells in order to graft them in muscular tissue, such as the heart to help for heart diseases.

**Supplementary Materials:** The following are available online at <https://www.mdpi.com/article/10.3390/surfaces4040026/s1>, Figure S1. Survey regions of modified PET. (a) PET-DMA, (b) PET-DMA-PHEMA-I, and (c) PET-DMA-PHEMA-I-FBN0.5, Figure S2. High resolution O1s regions from (a) PET, and (b) PET-DMA-PHEMA, Figure S3. High resolution N1s regions from (a) PET-DMA, (b) PET-DMA-PHEMA-I, and (c) PET-DMA-PHEMA-I-FBN5, Figure S4. S2p, narrow regions from PET-DMA-PHEMA-I-FBN prepared with an initial fibronectin concentration of 0.5 and 5  $\mu\text{g}/\text{mL}$ .

**Author Contributions:** Conceptualization, M.M.C.; Data curation, S.S., D.G. and E.C.; Formal analysis, S.S., D.G. and E.C.; Funding acquisition, D.K.A. and M.M.C.; Investigation, S.S., E.C. and A.L.; Methodology, S.S., E.C., A.L. and D.K.A.; Supervision, A.S. and D.K.A.; Validation, A.L. and A.S.; Visualization, A.L.; Writing—original draft, S.S.; Writing—review & editing, S.S., D.G., E.C., A.L., A.S., D.K.A. and M.M.C. All authors have read and agreed to the published version of the manuscript.

**Funding:** This research was funded by the Indo-French Centre for the Promotion of Advanced Research (IFCPAR), grant number 4705-2.

**Institutional Review Board Statement:** Not applicable.

**Informed Consent Statement:** Not applicable.

**Data Availability Statement:** Raw data not available in any server but available upon request to the corresponding author.

**Acknowledgments:** Inverted microscopic analysis were performed on the “Plateau imagerie”, of Unit of Functional and Adaptive Biology (BFA), Université de Paris, Paris, France.

**Conflicts of Interest:** The authors declare no conflict of interest.

## References

1. Schwartz, M.A. Integrins and extracellular matrix in mechanotransduction. *Cold Spring Harb. Perspect Biol.* **2010**, *2*, a005066. [[CrossRef](#)]
2. Srivastava, N.; James, J.; Narayan, K.S. Morphology and electrostatics play active role in neuronal differentiation processes on flexible conducting substrates. *Organogenesis* **2014**, *10*, 1–5. [[CrossRef](#)] [[PubMed](#)]
3. Nune, M.; Manchineella, S.; Govindaraju, T.; Narayan, K.S. Melanin incorporated electroactive and antioxidant silk fibroin nanofibrous scaffolds for nerve tissue engineering. *Mater. Sci. Eng. C* **2019**, *94*, 17–25. [[CrossRef](#)] [[PubMed](#)]
4. Park, J.H.; Park, J.U.; Chang, H. Advances in Biomaterials for Breast Reconstruction. *Appl. Sci.* **2021**, *11*, 7493. [[CrossRef](#)]
5. Balakin, S.; Ibarlucea, B.; Belyaev, D.; Baraban, L.; Hänsel, S.; Maitz, M.; Werner, C.; Cuniberti, G. Hemocompatible Electrochemical Sensors for Continuous Monitoring of Blood Parameters. *Eng. Proc.* **2021**, *6*, 19. [[CrossRef](#)]
6. Kou, L.; Yao, Q.; Zhang, H.; Chu, M.; Bhutia, Y.D.; Chen, R.; Ganapathy, V. Transporter-targeted nano-sized vehicles for enhanced and site-specific drug delivery. *Cancers* **2020**, *12*, 2837. [[CrossRef](#)]
7. Chung, S.; King, M.W. Design concepts and strategies for tissue engineering scaffolds. *Biotechnol. Appl. Biochem.* **2011**, *58*, 423–438. [[CrossRef](#)]
8. Ng, K.; Gao, B.; Yong, K.W.; Li, Y.; Shi, M.; Zhao, X.; Li, Z.; Zhang, X.; Pinguan-Murphy, B.; Yang, H.; et al. Paper-based cell culture platform and its emerging biomedical applications. *Mater. Today* **2017**, *20*, 32–44. [[CrossRef](#)]
9. Brown, R.A.; Phillips, J.B. Cell Responses to Biomimetic Protein Scaffolds Used in Tissue Repair and Engineering. *Int. Rev. Cytol.* **2007**, *262*, 75–150.
10. Zhang, X.; Xu, B.; Puperi, D.S.; Yonezawa, A.L.; Wu, Y.; Tseng, H.; Grande-Allen, K.J. Integrating valve-inspired design features into poly (ethylene glycol) hydrogel scaffolds for heart valve tissue engineering. *Acta Biomater.* **2015**, *14*, 11–21. [[CrossRef](#)]
11. Abdul Samat, A.; Abdul Hamid, Z.A.; Jaafar, M.; Yahaya, B.H. Mechanical Properties and In Vitro Evaluation of Thermoplastic Polyurethane and Polylactic Acid Blend for Fabrication of 3D Filaments for Tracheal Tissue Engineering. *Polymers* **2021**, *13*, 3087. [[CrossRef](#)]
12. Beldjilali-Labro, M.; Garcia Garcia, A.; Farhat, F.; Bedoui, F.; Grosset, J.F.; Dufresne, M.; Legallais, C. Biomaterials in tendon and skeletal muscle tissue engineering: Current trends and challenges. *Materials* **2018**, *11*, 1116. [[CrossRef](#)]
13. Vasiliadis, A.V.; Katakalos, K. The Role of Scaffolds in Tendon Tissue Engineering. *J. Funct. Biomater.* **2020**, *11*, 78. [[CrossRef](#)]
14. Zhao, Y.; Li, Y.; Peng, X.; Yu, X.; Cheng, C.; Yu, X. Feasibility study of oxidized hyaluronic acid cross-linking acellular bovine pericardium with potential application for abdominal wall repair. *Int. J. Biol. Macromol.* **2021**, *184*, 831–842. [[CrossRef](#)]
15. Brown, B.N.; Badylak, S.F. Extracellular matrix as an inductive scaffold for functional tissue reconstruction. *Transl. Res.* **2013**, *163*, 268–285. [[CrossRef](#)] [[PubMed](#)]
16. Mecham, R.P. Overview of extracellular matrix. *Curr. Protoc. Cell Biol.* **2012**, *57*, 10.1.1–10.1.16. [[CrossRef](#)]
17. Hussey, G.S.; Dziki, J.L.; Badylak, S.F. Extracellular matrix-based materials for regenerative medicine. *Nat. Rev. Mater.* **2018**, *3*, 159–173. [[CrossRef](#)]
18. Hynes, R.O.; Naba, A. Overview of the matrisome—An inventory of extracellular matrix constituents and functions. *Cold Spring Harb. Perspect Biol.* **2012**, *4*, a004903. [[CrossRef](#)] [[PubMed](#)]
19. Statzer, C.; Ewald, C.Y. The extracellular matrix phenome across species. *Matrix Biol. Plus* **2020**, *8*, 100039. [[CrossRef](#)] [[PubMed](#)]
20. Lu, P.; Takai, K.; Weaver, V.M.; Werb, Z. Extracellular matrix degradation and remodeling in development and disease. *Cold Spring Harb. Perspect Biol.* **2011**, *3*, a005058. [[CrossRef](#)]
21. Winkler, J.; Abisoye-Ogunniyan, A.; Metcalf, K.J.; Werb, Z. Concepts of extracellular matrix remodelling in tumour progression and metastasis. *Nat. Commun.* **2020**, *11*, 5120. [[CrossRef](#)] [[PubMed](#)]
22. Singh, A.; Zakaria, S.; Joshi, N.; Jha, P.; Decorse, P.; Lecoq, H.; Lau-Truong, S.; Jouini, M.; Aswal, D.K.; Chehimi, M.M. Electrochemical investigation of free-standing polypyrrole–silver nanocomposite films: A substrate free electrode material for supercapacitors. *RSC Adv.* **2013**, *3*, 24567–24575. [[CrossRef](#)]
23. Lo, M.; Seydou, M.; Bensghaier, A.; Pires, R.; Ngingue-Sall, D.; Aaron, J.J.; Mekhalif, Z.; Delhalle, J.; Chehimi, M.M. Polypyrrole-wrapped carbon nanotube composite films coated on diazonium-modified flexible ITO sheets for the electroanalysis of heavy metal ions. *Sensors* **2020**, *20*, 580. [[CrossRef](#)] [[PubMed](#)]
24. Fukuda, K.; Yu, K.; Someya, T. The future of flexible organic solar cells. *Adv. Energy Mater.* **2020**, *10*, 2000765. [[CrossRef](#)]
25. Gooding, J.J.; Ciampi, S. The molecular level modification of surfaces: From self-assembled monolayers to complex molecular assemblies. *Chem. Soc. Rev.* **2011**, *40*, 2704–2718. [[CrossRef](#)]
26. Mousli, F.; Snoussi, Y.; Khalil, A.M.; Jlassi, K.; Mekki, A.; Chehimi, M.M. Surface Modification of Polymeric Substrates with Photo- and Sonochemically Designed Macromolecular Grafts. In *Surface Modification of Polymers: Methods and Applications*; Pinson, J., Thiry, D., Eds.; Wiley-VCH: Weinheim, Germany, 2019; pp. 273–315.
27. Hetemi, D.; Noël, V.; Pinson, J. Grafting of diazonium salts on surfaces: Application to biosensors. *Biosensors* **2020**, *10*, 4. [[CrossRef](#)]
28. Amani, H.; Arzaghi, H.; Bayandori, M.; Dezfali, A.S.; Pazoki-Toroudi, H.; Shafiee, A.; Moradi, L. Controlling cell behavior through the design of biomaterial surfaces: A focus on surface modification techniques. *Adv. Mater. Interfaces* **2019**, *6*, 1900572. [[CrossRef](#)]

29. Zoppe, J.O.; Ataman, N.C.; Mocny, P.; Wang, J.; Moraes, J.; Klok, H.A. Surface-initiated controlled radical polymerization: State-of-the-art, opportunities, and challenges in surface and interface engineering with polymer brushes. *Chem. Rev.* **2017**, *117*, 1105–1318. [[CrossRef](#)]
30. Bensghaïer, A.; Mousli, F.; Lamouri, A.; Postnikov, P.S.; Chehimi, M.M. The Molecular and Macromolecular Level of Carbon Nanotube Modification Via Diazonium Chemistry: Emphasis on the 2010s Years. *Chem. Afr.* **2020**, *3*, 535–569. [[CrossRef](#)]
31. Chehimi, M.M. (Ed.) *Aryl Diazonium Salts: New Coupling Agents in Polymer and Surface Science*; Wiley-VCH: Weinheim, Germany, 2012.
32. Bélanger, D.; Pinson, J. Electrografting: A powerful method for surface modification. *Chem. Soc. Rev.* **2011**, *40*, 3995–4048. [[CrossRef](#)] [[PubMed](#)]
33. Gautier, C.; Lopez, I.; Breton, T. A post-functionalization toolbox for diazonium (electro)-grafted surfaces: Review of the coupling methods. *Mater. Adv.* **2021**, *2*, 2773–2810. [[CrossRef](#)]
34. Ben Slama, R.; Mrabet, B.; Bakhrouf, A.; Salmi, Z.; Bakas, I.; Chehimi, M.M. Polymer/silver hybrid thin films for anti-pathogenic bacterial applications. *Surf. Innov.* **2015**, *3*, 103–114. [[CrossRef](#)]
35. Mahjoubi, H.; Buck, E.; Manimunda, P.; Farivar, R.; Chromik, R.; Murshed, M.; Cerruti, M. Surface phosphonation enhances hydroxyapatite coating adhesion on polyetheretherketone and its osseointegration potential. *Acta Biomater.* **2017**, *47*, 149–158. [[CrossRef](#)] [[PubMed](#)]
36. Boccafoschi, F.; Fusaro, L.; Botta, M.; Ramella, M.; Chevallier, P.; Mantovani, D.; Cannas, M. Arginine-glycine-glutamine and serine-isoleucine-lysine-valine-alanine-valine modified poly(l-lactide) films: Bioactive molecules used for surface grafting to guide cellular contractile phenotype. *Biointerphases* **2014**, *9*, 029002. [[CrossRef](#)] [[PubMed](#)]
37. Gam-Derouich, S.; Mahouche-Chergui, S.; Turmine, M.; Piquemal, J.Y.; Hassen-Chehimi, D.B.; Omastová, M.; Chehimi, M.M. A versatile route for surface modification of carbon, metals and semi-conductors by diazonium salt-initiated photopolymerization. *Surf. Sci.* **2011**, *605*, 1889–1899. [[CrossRef](#)]
38. Zare, M.; Bigham, A.; Zare, M.; Luo, H.; Rezvani Ghomi, E.; Ramakrishna, S. pHEMA: An Overview for Biomedical Applications. *Int. J. Mol. Sci.* **2021**, *22*, 6376. [[CrossRef](#)]
39. Yang, J.; Shen, M.H. Polyethylene glycol-mediated cell fusion. *Methods Mol. Biol.* **2006**, *325*, 59–66.
40. Legeay, G.; Coudreuse, A.; Poncin-Epaillard, F.; Herry, J.M.; Bellon-Fontaine, M.N. Surface engineering and cell adhesion. *J. Adhes. Sci. Technol.* **2010**, *24*, 2301–2322. [[CrossRef](#)]